

# Classical solutions of the Gravitating Abelian Higgs Model.

Y. Brihaye, M. Lubo

Faculté des Sciences, Université de Mons-Hainaut,

B-7000 MONS, Belgium.

## Abstract

We consider the classical equations of the gravitating Abelian-Higgs model in an axially symmetric ansatz. More properties of the solutions of these equations (the Melvin and the sting branches) are presented. These solutions are also constructed for winding numbers  $N = 2$ . It is shown that these vortices exist in attractive and repulsive phases, separated by the value of the Higgs coupling constant parameter leading to self-dual equations.

# 1 Introduction

Most of the well known classical solutions in field theory are constructed in Minkowski space. Taking into account gravity, one recovers them as limiting cases but some new solutions appear which cannot be reached continuously from the existing one in flat space. Such a situation occurs when one considers an Abelian-Higgs system. Imposing cylindrical symmetry, one finds that there is only one solution : the cosmic string [2]. When gravity sets in, this configuration experiences a deformation which manifests itself as a conical singularity. As the angular deficit vanishes with the coupling constant measuring the gravitational interaction, this solution evolves smoothly from flat to curved space. It has been shown recently that there exists another solution exhibiting axial symmetry in the gravitating Abelian-Higgs system [1]. The profiles of axial functions parametrizing the metric and the matter fields have been obtained for a unit winding number.

In this work, we first address the question of the link between the masses (inertial mass and Tolman mass) of the new configurations and the parameters of the model (the ratio  $\alpha$  of the vector mass by the scalar mass on one side, the product  $\gamma$  of the Newton constant by the square of the Higgs-field's expectation value on the other side). They are contrasted with those of the corresponding gravitating string. We then turn to configurations with higher winding numbers and analyze their stability. The phenomenon first pointed out in [7] is present for the gravitating strings and for the new (Melvin-like) solution.

In a certain domain of the parameter space, the solution becomes closed i.e. defined within a maximal radius of the axial variable. We also investigate the dependence of this maximal radius versus  $\alpha$  and  $\gamma$ .

## 2 The equations.

We consider the gravitating Abelian Higgs model in four dimensions. It is described by the action

$$S = \int d^4x \sqrt{-g} \mathcal{L} \quad (1)$$

$$\mathcal{L} = \frac{1}{2} D_\mu \phi D^\mu \phi^* - \frac{1}{4} F_{\mu\nu} F^{\mu\nu} - \frac{\lambda}{4} (\phi^* \phi - v^2)^2 + \frac{1}{16\pi G} R \quad (2)$$

where  $D_\mu = \nabla_\mu - ieA_\mu$  is the gauge covariant derivative,  $A_\mu$  is the gauge potential of the U(1) gauge symmetry,  $F_{\mu\nu}$  is the corresponding field strength and  $\phi$  is a complex scalar field with vacuum expectation value  $v$ . The usual Ricci scalar is denoted  $R$ . We use the same notations as [1].

In the following we study the classical equations of the above field theory within the cylindrically symmetric ansatz. The metric and matter fields are parametrized in terms of four functions of the cylindrical radial variable  $r$  :

$$ds^2 = N^2(r) dt^2 - dr^2 - L^2(r) d\phi^2 - N^2(r) dz^2 \quad (3)$$

$$\phi = v f(r) e^{in\phi} \quad (4)$$

$$A_\mu dx^\mu = \frac{1}{e} (n - P(r)) d\phi \quad (5)$$

Here  $N, L, P, f$  are the four radial functions of  $r$ ,  $n$  is an integer indexing the vorticity of the Higgs field around the  $x_3$  axis. In [1] it was shown that the above ansatz consistently leads to the following system of equations for the functions  $N, L, P, f$  :

$$\frac{(LNN')'}{N^2L} = \gamma \left( \frac{P'^2}{2\alpha L^2} - \frac{1}{4} (1 - f^2)^2 \right) \quad (6)$$

$$\frac{(N^2L')'}{N^2L} = -\gamma \left( \frac{P'^2}{2\alpha L^2} + \frac{P^2 f^2}{L^2} + \frac{1}{4} (1 - f^2)^2 \right) \quad (7)$$

$$\frac{L}{N^2} \left( \frac{N^2 P'}{L} \right)' = \alpha f^2 P \quad (8)$$

$$\frac{(N^2 L f')'}{N^2 L} = f(f^2 - 1) + f \frac{p^2}{L^2} \quad (9)$$

where  $\alpha = e^2/\lambda$  and  $\gamma = 8\pi Gv^2$  are the physical constants. The dimensionless coordinate  $x = \sqrt{\lambda v^2}$  has been used and the primes mean derivatives with respect to  $x$ . The problem posed by the differential equations is then further specified by the following set of boundary conditions

$$N(0) = 1 \quad , \quad N'(0) = 0 \quad (10)$$

$$L(0) = 0 \quad , \quad L'(0) = 1 \quad (11)$$

$$P(0) = n \quad , \quad \lim_{x \rightarrow \infty} P(x) = 0 \quad (12)$$

$$f(0) = 0 \quad , \quad \lim_{x \rightarrow \infty} f(x) = 1 \quad (13)$$

which are necessary to guarantee the regularity of the configuration at the origin and the finiteness of the inertial mass defined next.

The different solutions of the system can be characterized by the inertial mass per unit length

$$\mathcal{M}_{in} = \int \sqrt{-g_3} T_0^0 dx_1 dx_2 \quad (14)$$

and by the Tolman mass per unit length

$$\mathcal{M}_{to} = \int \sqrt{-g_4} T_\mu^\mu dx_1 dx_2 \quad (15)$$

In the cylindrically symmetric ansatz used and with the dimensionless variable  $x = \sqrt{\lambda v r}$  the two quantities above are given by the following radial integrals

$$\begin{aligned} G\mathcal{M}_{in} &\equiv \frac{\gamma}{8} M_{in} \\ &= \frac{\gamma}{8} \int_0^\infty dx N L \left( (f')^2 + \frac{(P')^2}{\alpha L^2} + \frac{P^2 f^2}{L^2} + \frac{1}{2}(1 - f^2)^2 \right) \end{aligned} \quad (16)$$

$$\begin{aligned} G\mathcal{M}_{to} &\equiv \frac{\gamma}{2} M_{to} \\ &= \frac{\gamma}{2} \int_0^\infty dx N^2 L \left( \frac{(P')^2}{2\alpha L^2} - \frac{1}{4}(1 - f^2)^2 \right) \end{aligned} \quad (17)$$

The integral determining the Tolman mass can be evaluated by means of equation (6) and is given by the following limit

$$G\mathcal{M}_{to} = \frac{1}{2} \lim_{x \rightarrow \infty} (L N N') \quad (18)$$

### 3 Discussion of the global solutions.

Let us first discuss the solutions of the system (6), (9) which are regular on  $[0, \infty]$ , i.e. when  $N, L$  have no zero on this interval.

#### 3.1 The string branch.

In the flat case  $\gamma = 0$ , equations (6)-(9) admit the celebrated Nielsen-Olesen [2] string as solution :

$$N = 1 \quad , \quad L = x \quad , \quad P = P_{no}(x) \quad , \quad f = f_{no}(x) \quad (19)$$

where  $P_{no}$  and  $f_{no}$  are determined numerically. When the parameter  $\gamma$  is increased from zero, the solution (19) gets progressively deformed by gravity. In particular the functions  $N, L$  become more complicated. Asymptotically they obey the following behaviour

$$N(x \rightarrow \infty) = a \quad (20)$$

$$L(x \rightarrow \infty) = bx + c \quad , \quad b > 0 \quad (21)$$

here  $a, b, c$  are constants depending on  $\alpha, \gamma$ . According to (18), the Tolman mass vanishes.

For fixed  $\alpha$ , the set of solutions obtained by varying  $\gamma$  (or vice versa) assemble into a branch of solutions called, after [1], the string branch. They exist as global solution on  $x \in [0, \infty]$  up to a critical value  $\gamma_{cr}(\alpha)$  (or, equivalently if  $\gamma$  is fixed up to  $\alpha_{er}(\gamma)$ ) which is reached when the parameter  $b$  (defined in (21)) becomes zero (solutions corresponding to  $\gamma > \gamma_{cr}$  and  $b < 0$  will be the object of the next section). This phenomenon is illustrated by Fig.1 for  $\alpha = 1.0$  (solid lines) and  $\alpha = 3.0$  (dashed lines).

The figure further indicates that the inertial mass  $M_{in}$  increases slightly with  $\gamma$  while the parameter  $b$  decreases linearly with  $\gamma$ . Moreover, the critical value

$\gamma_a(\alpha)$  increases with  $\gamma$ , e.g.

$$\gamma_{cr}(1.0) \approx 1.66 \quad (22)$$

$$\gamma_{cr}(2.0) = 2.0 \quad (23)$$

$$\gamma_{cr}(3.0) \approx 2.2 \quad (24)$$

The case  $\alpha = 2$  possesses further algebraical properties because there exist underlying self-dual (first order) equations implying the full equations (6), (9). In particular we have in this case

$$N(x) = 1. \quad , \quad M_{in}(\gamma) = 1 \quad (25)$$

$$a = 1 \quad , \quad b = 1 - \frac{\gamma}{2} \quad , \quad \gamma_{cr}(2) = 2 \quad (26)$$

### 3.2 The Melvin branch.

As discovered by [1], any global solution on the string branch possesses a shadow solution. This second set of global solutions of Eqs (6)-(9) assemble into a branch named, after [1], the Melvin branch. The profile of a solution on the Melvin branch is presented in Fig. 2 for typical values of the parameters  $\alpha = 1.8, \gamma = 1$ .

In contrast to (20), (21), the asymptotic behaviour of the Melvin-branch solutions is such that

$$N(x \rightarrow \infty) \simeq Ax^{2/3} \quad (27)$$

$$L(x \rightarrow \infty) \simeq Bx^{-1/3} \quad (28)$$

As a consequence the Tolman mass is not zero any longer :

$$GM_{to} = \frac{1}{2} \lim_{x \rightarrow \infty} (LNN') = \frac{1}{3} A^2 B \quad (29)$$

The inertial and Tolman masses of the string and Melvin branches are plotted on Fig. 3 as functions of  $\alpha$  and for  $\gamma = 1$  (in this case the critical value of  $\alpha$  is  $\alpha_{er} \approx 0.155$ ). The figure clearly indicates that both (inertial and Tolman) masses

are higher for the Melvin branch than for the string branch. In the limit  $\alpha \rightarrow \alpha_{cr}$ , the numerical analysis confirms that the inertial masses (and also the Tolman masses) of the string and Melvin branches tend to a common value (in the case of the Tolman mass, this value is zero).

The way the different radial functions associated with the two solutions approach each other in the limit  $\alpha \rightarrow \alpha_{cr}$  is illustrated by Figs 4 and 5 where the profiles of the functions are presented respectively for  $\alpha = 0.2$  and  $\alpha = 0.16$ . In particular, it is seen on the figures that the matter functions  $f, P$  of the string branch deviate rather slowly from their counterparts of the Melvin branch.

The evolution of the masses  $M_{in}, M_{to}$  for  $\gamma \rightarrow 0$  on the Melvin branch is summarized by Fig. 6. The radial integral defining these quantities clearly diverges when  $\gamma$  approaches zero but the Einstein-Maxwell equations can be recovered from Eqs. (6)-(9) by rescaling the radial variable  $x$  and the function  $L(x)$  according to

$$x = \sqrt{\gamma}y \quad , \quad L = \sqrt{\frac{\gamma}{\alpha}}\tilde{L} \quad (30)$$

and setting  $\gamma = 0$  afterwards. Equation (9) then decouples and the remaining equations are the Einstein-Maxwell equations in the axially symmetric ansatz. The profile of the Melvin solution is illustrated on Fig. 7. It has

$$G\mathcal{M}_{in} = \frac{1}{4} \quad (31)$$

independently of  $\alpha$ .

This situation is somehow reminiscent to the case of the gravitating sphaleron solution of the Einstein-Weinberg-Salam equation (EWS) [3], [4]. The role played here by the flat Nielsen Olesen is played in EWS equation by the flat klinkhamer-Manton Sphaleron [5] while the role of the Melvin solution on the top of the upper branch is played by the first solution of the Bartnik-McKinnon series of solutions [6]. However, unlike in the present theory, the transition from the sphaleron to the Bartnik-Mc Kinnon solutions in the EWS model is smooth [4].

### 3.3 Solutions of vorticity $> 1$ .

Coming back to the flat Nielsen-Olesen equations, we know that solutions of vorticity  $n$  can be constructed while imposing the following boundary conditions on  $P(x)$  :

$$P(0) = n \quad , \quad P(\infty) = 0 \quad (32)$$

Denoting by  $M(n)$  the classical energy of the Nielsen-Olesen solution of vorticity  $n$ , one of the distinguished feature of the self dual case ( $\alpha = 2$ ) is the mass relation

$$M(n) = nM(1) \quad (33)$$

It is therefore a natural problem to check if the relation above still holds in presence of gravity. We did so by choosing  $\gamma = 1$  and by studying the inertial mass (which directly generalize the classical energy of the flat case) for the values of  $\alpha$  close to  $\alpha = 2$ . These results are presented on Fig. 8. The quantities  $M_{in}(1)$  and  $\frac{1}{2}M_{in}(2)$  cross at the self dual point  $\alpha = 2$  and their behaviour demonstrates that the Rebbi-Jacobs phenomenon [7] also holds when gravity is added. Namely for  $\alpha > 2$  (resp.  $\alpha < 2$ ) the binding energy of the  $n = 2$  string solution is negative (resp. positive).

## 4 Closed solutions.

As said above, the critical value  $\gamma_{cr}(\alpha)$  (or equivalently  $\alpha_{cr}(\gamma)$ ) is determined when the slope parameter  $b$  of the function  $L$  is zero. For  $\gamma > \gamma_u(\alpha)$  (or  $\alpha < \alpha_u(\gamma)$ ) the string and Melvin branches of solution continue to exist but they are not any longer available as regular solution for  $x \in [0, \infty]$ . The fact that one of the functions  $N$  or  $L$  has a zero at, say  $x = x_0$ , leads to a singular point of Eq. (6) or (7). Correspondingly the solution can only be constructed for  $x \in [0, x_0]$ .

The inertial masses of the solutions continuing the Melvin and string branches for  $\alpha < \alpha_{cr}$  are presented in Fig. 3. Clearly, the closed solution having the lowest



mass is the continuation (for  $\alpha < \alpha_{cr}$ ) of the Melvin branch. In [1], it is called the Kasner branch. An example of such a solution is presented on Fig. 10 for  $\gamma = 1, \alpha = 0.14$ . It terminates at  $x_0 \simeq 26$ . The evolution of  $x_0$ , the maximal value of  $n$ , in function of  $\alpha$  is presented on Fig. 11.

## 5 Conclusion and outlook

We have seen that, for a fixed  $\alpha$ , the mass of a string grows with  $\gamma$  while the Melvin-like configuration display the opposite behaviour. This results in the existence of a critical value  $\alpha_0$  such that the new solution is heavier (resp. lighter) than a string for  $\alpha > \alpha_0$  (resp.  $\alpha < \alpha_0$ ). The numerical calculations show that  $\alpha_0 = 0.5$ . Another particular value of interest is  $\alpha = 2$ , for which there exists first order equations implying the classical equations (this is self duality). For  $\alpha > 2$  the Melvin-like configurations have a negative binding energy and, likely, are stable versus decaying into several solutions of unit vorticity. This is also the case with cosmic string solutions. So the kind of solutions considered here obey the Jacobs-Rebbi [7] phenomenon on both sides of the self dual point  $\alpha = 2$ . We also studied how the radius of the closed solutions grows with  $\alpha$ .

The Melvin-like solution raises many questions. A first one is a full understanding of its geometry [8]. A second one is the elaboration of a plausible mechanism for the generation of such a configuration. For example, cosmic strings can be formed during a phase transition. This scenario seems conceptually difficult to implement here since one would have to perform quantum field theory at finite temperature and on a curved background.

Cosmic string can also be formed by the collision of two monopoles. If the Melvin-type configuration has to be generated in this way, then the problem is a technical one since one has to solve the field equations for a fully time and position dependant ansatz. If any of these two mechanisms takes place with a reasonable efficiency, then the new solution is likely to play a significant role in

cosmology, like its string cousins whose possible implications ranges from density generation to baryogenesis [9].

The kind of calculations reported here could be extended to other members of the Abelian models hierarchy[10] for which self dual equations are available as well. Lagrangians constructed by superposing a few members of the hierarchy could also be considered [11]; for such models, however, (and at least for flat space) only quasi self dual equations exist.

## References

- [1] M. Christensen, A.L. Larsen and Y. Verbin, Phys. Rev. D60 (1999) 12501-2.
- [2] H.B. Nielsen and P. Olesen, Nucl. Phys. B61 (1973) 45.
- [3] M.S. Volkov and D.V. Gal'tsov, Phys. Rep. 319 (1999) 1.
- [4] Y. Brihaye and M. Desoil, "Gravitating (bi)-Sphalerons", hep-th/0001100.
- [5] F.R. Klinkhamer and N.S. Manton, Phys. Rev. D30 (1984) 2212.
- [6] R. Bartnik and J. Mc Kinnon, Phys. Rev. Lett. 61 (1988) 141.
- [7] L. Jacobs and C. Rebbi, Phys. Rev. D19 (1979) 4486.
- [8] V. P. Frolov , W. Israel and W. G. Unruh, Phys. Rev. D39 (1989) 1084.
- [9] R. Jeannerot, Phys. Rev. Lett. 77 (1996) 3292.
- [10] J. Burzlaff, A. Chakrabarti and D. H. Tchrakian, J. Phys. A 27 (1994) 1617.
- [11] K. Arthur, Y. Brihaye and D. H. Tchrakian, Journ. Math. Phys. 39 (1998) 3031.

## Figures Captions

**Figure 1** The inertial mass  $M_{in}$  and the quantities  $a, b$  defined in (20), (21) as functions of  $\gamma$  and for  $\alpha = 1, 0$  (solid) and  $\alpha = 3.0$  (dashed).

**Figure 2** The profiles of the solution on the Melvin branch for  $\alpha = 1.8, \gamma = 1.0$ .

**Figure 3** The inertial mass  $M_{in}$ , the Tolman mass  $H_{to}$  and the quantities  $a, b$  of Eqs. (20), (21) as functions of  $\alpha$  (for  $\gamma = 1$ ) for the string (solid) and Melvin (dashed) solutions.

**Figure 4** The string (solid) and Melvin (dashed) solutions for  $\gamma = 1.0, \alpha = 0.2$ .

**Figure 5** The string (solid) and Melvin (dashed) solutions for  $\gamma = 1.0, \alpha = 0.16$ .

**Figure 6** The inertial mass  $M_{in}$  and Tolman mass  $M_{to}$  for the Melvin branches as functions of  $\gamma$  for  $\alpha = 1$ . The dashed lines represent the ratio  $M/\gamma$ .

**Figure 7** The approach of the Melvin solution ( $\gamma = 0$ ) by the solutions of the Melvin branch for decreasing values of  $\gamma$ .

**Figure 8** The quantity  $M_{in}(n)/n$  for  $n = 1$  (solid) and  $n = 2$  (dashed) in function of  $\alpha$  for  $\gamma = 1$ .

**Figure 9** The profiles of the solution on the Kasner branch for  $\gamma = 1, \alpha = 0.14$ . The function  $N$  crosses zero at  $x \approx 26$ .

**Figure 10** The evolution of the quantity  $x_{max}$  on the Kasner branch in function of  $\alpha$  and for  $\gamma = 1$ .

Figure 1

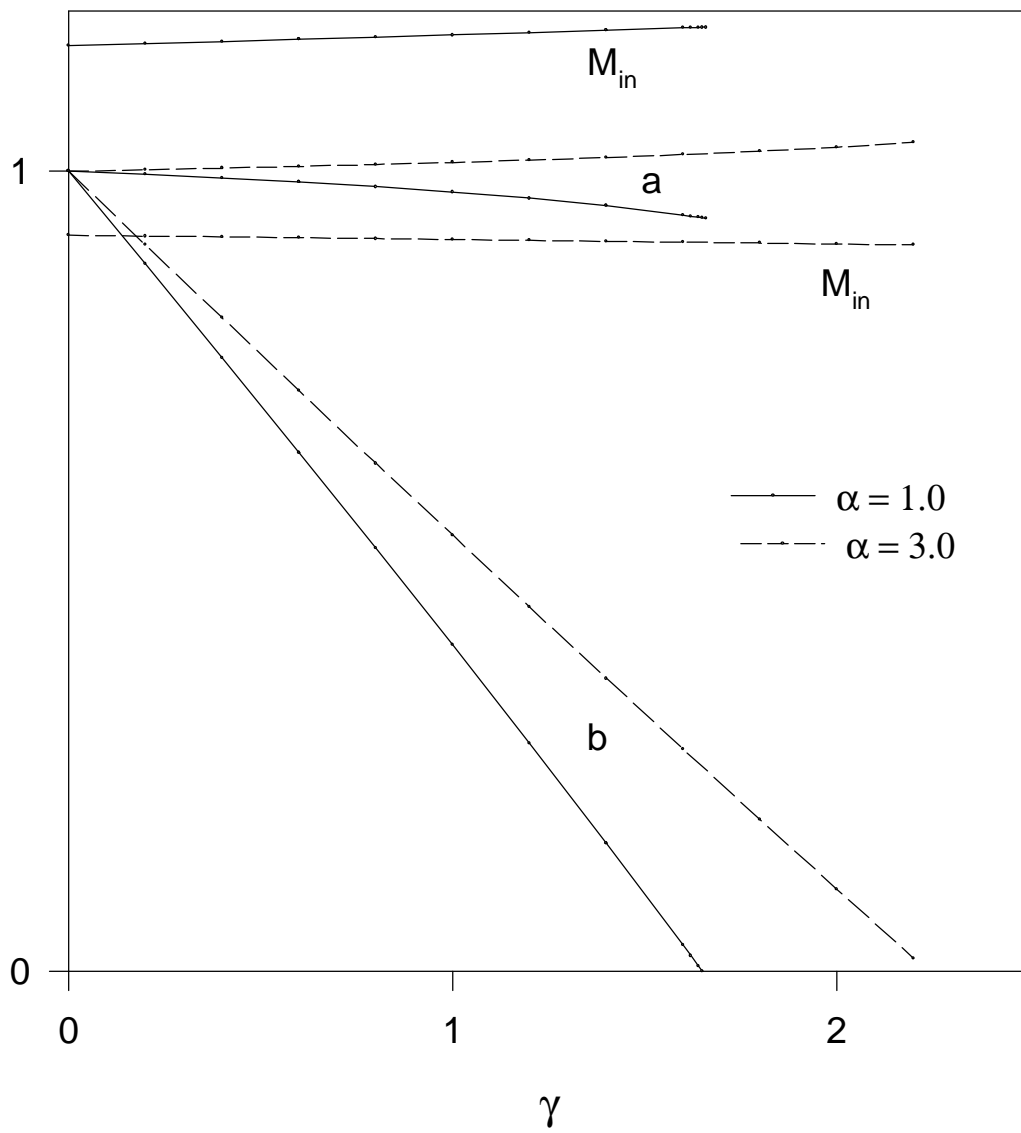


Figure 2

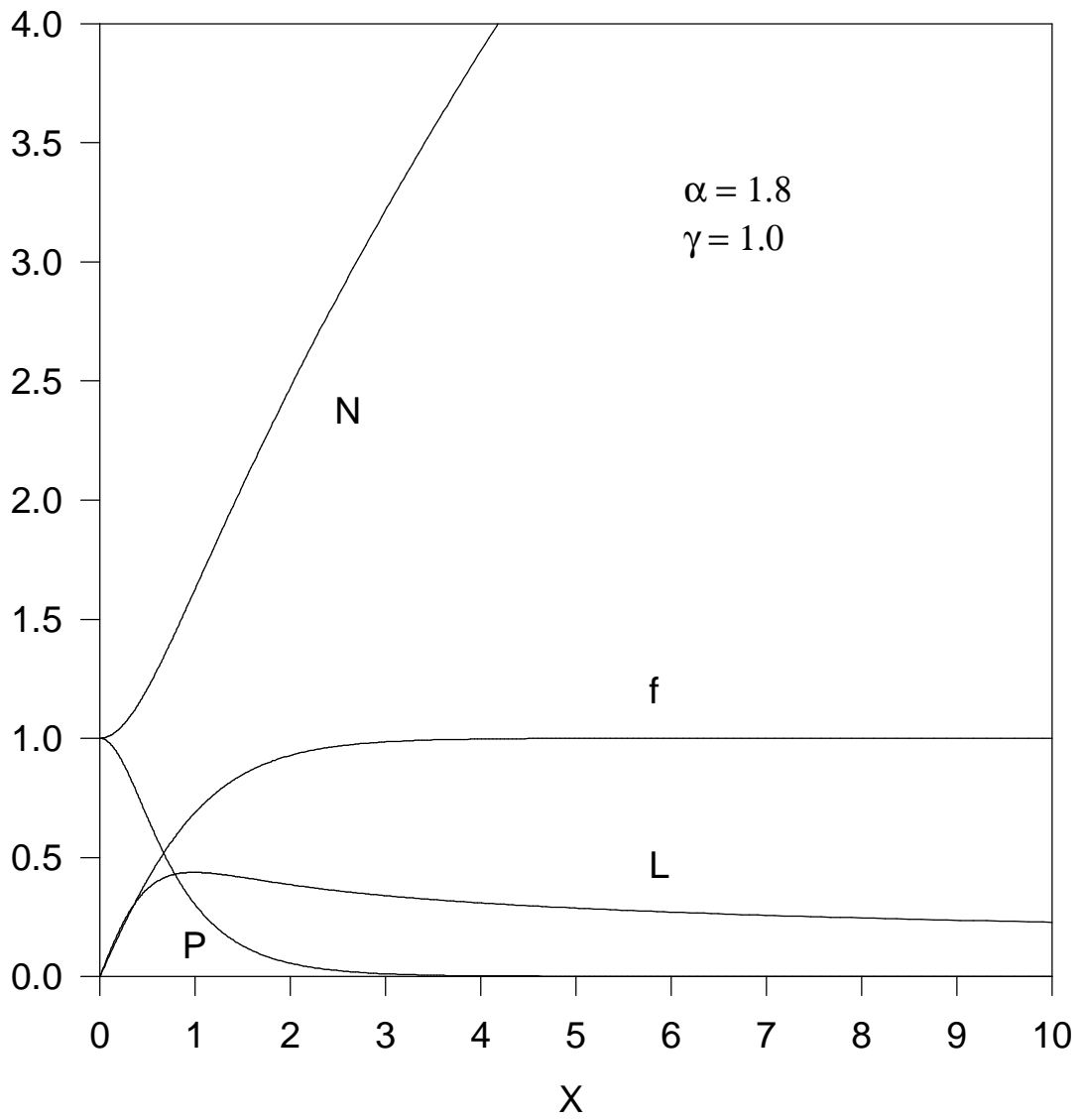


Figure 3

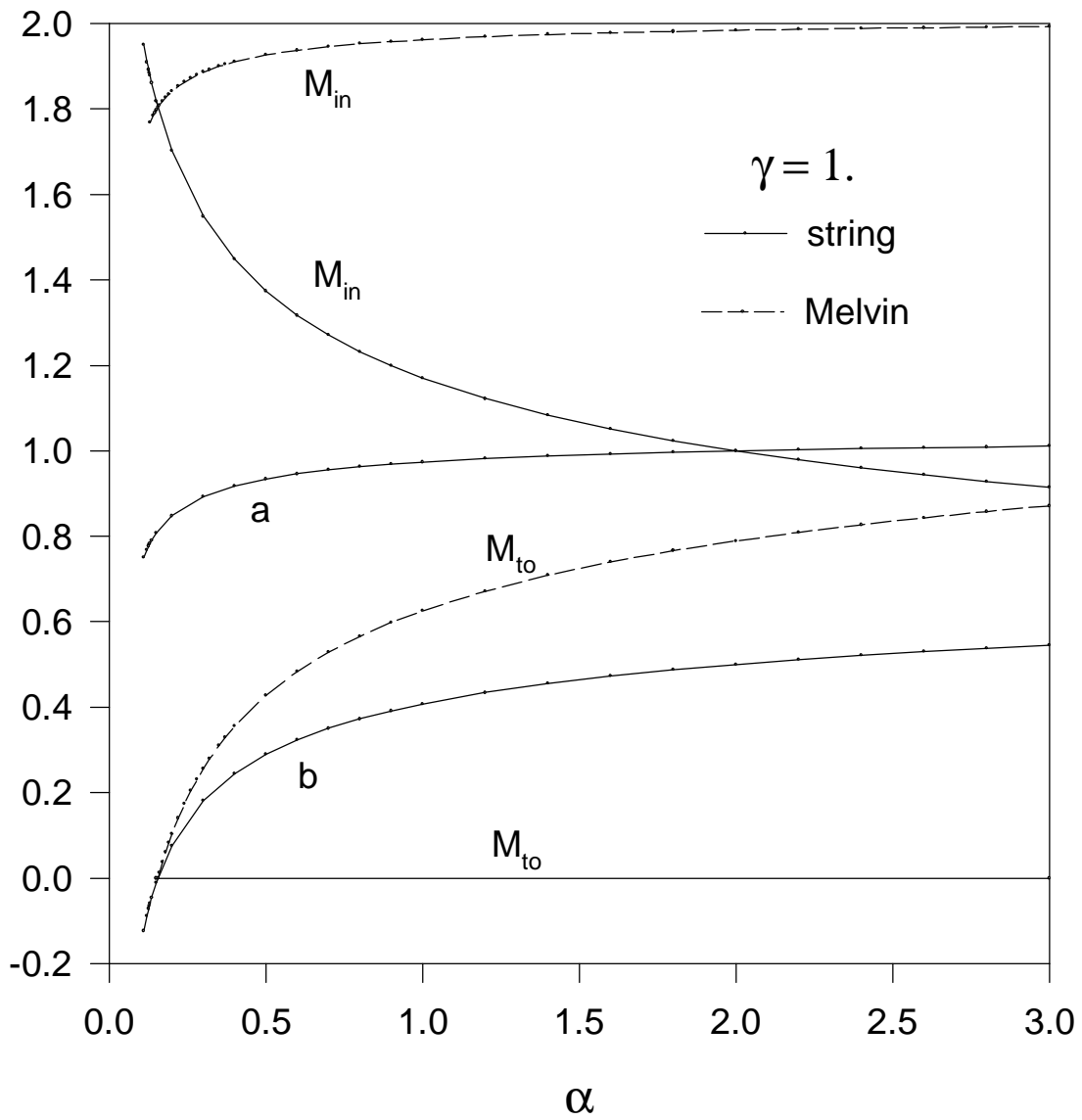
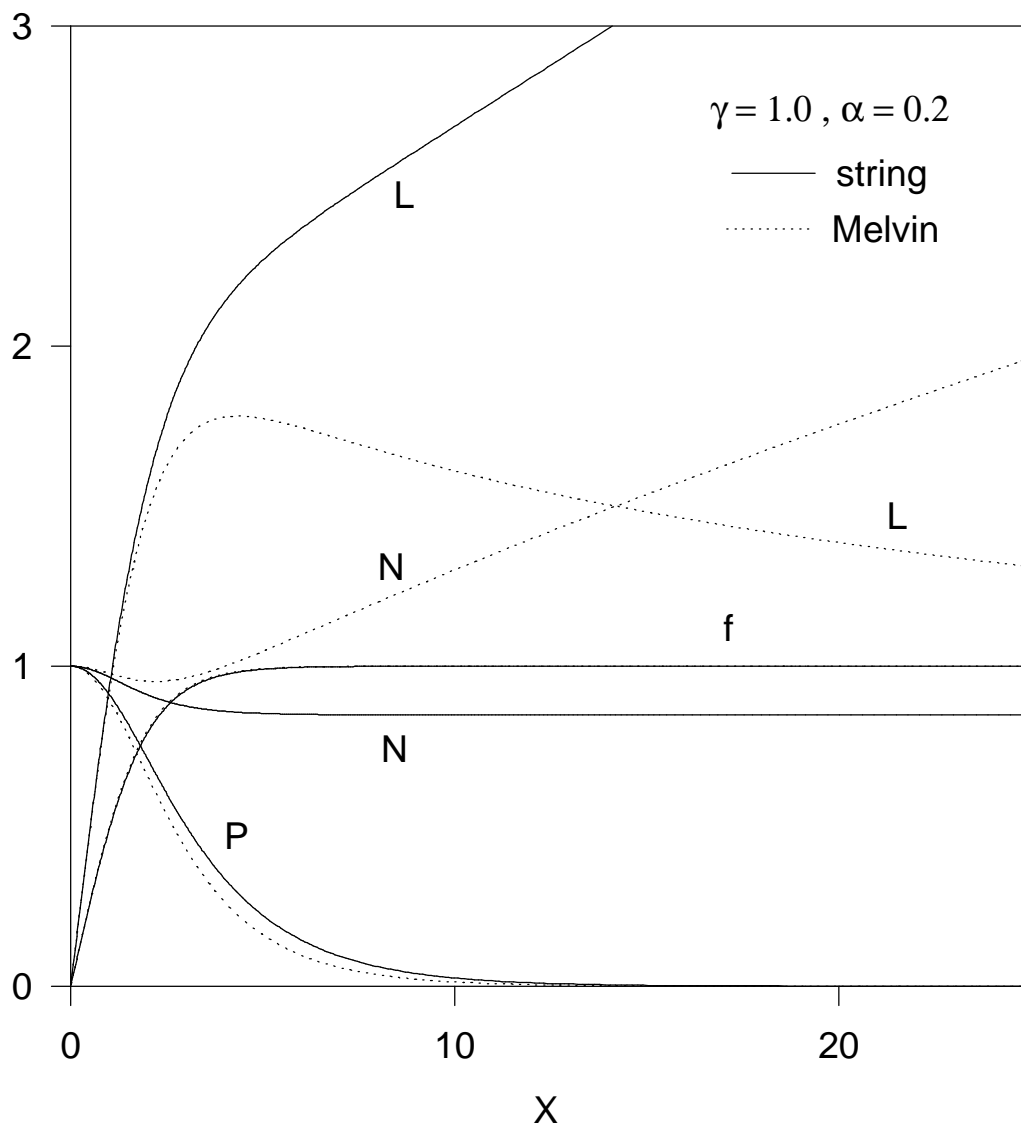
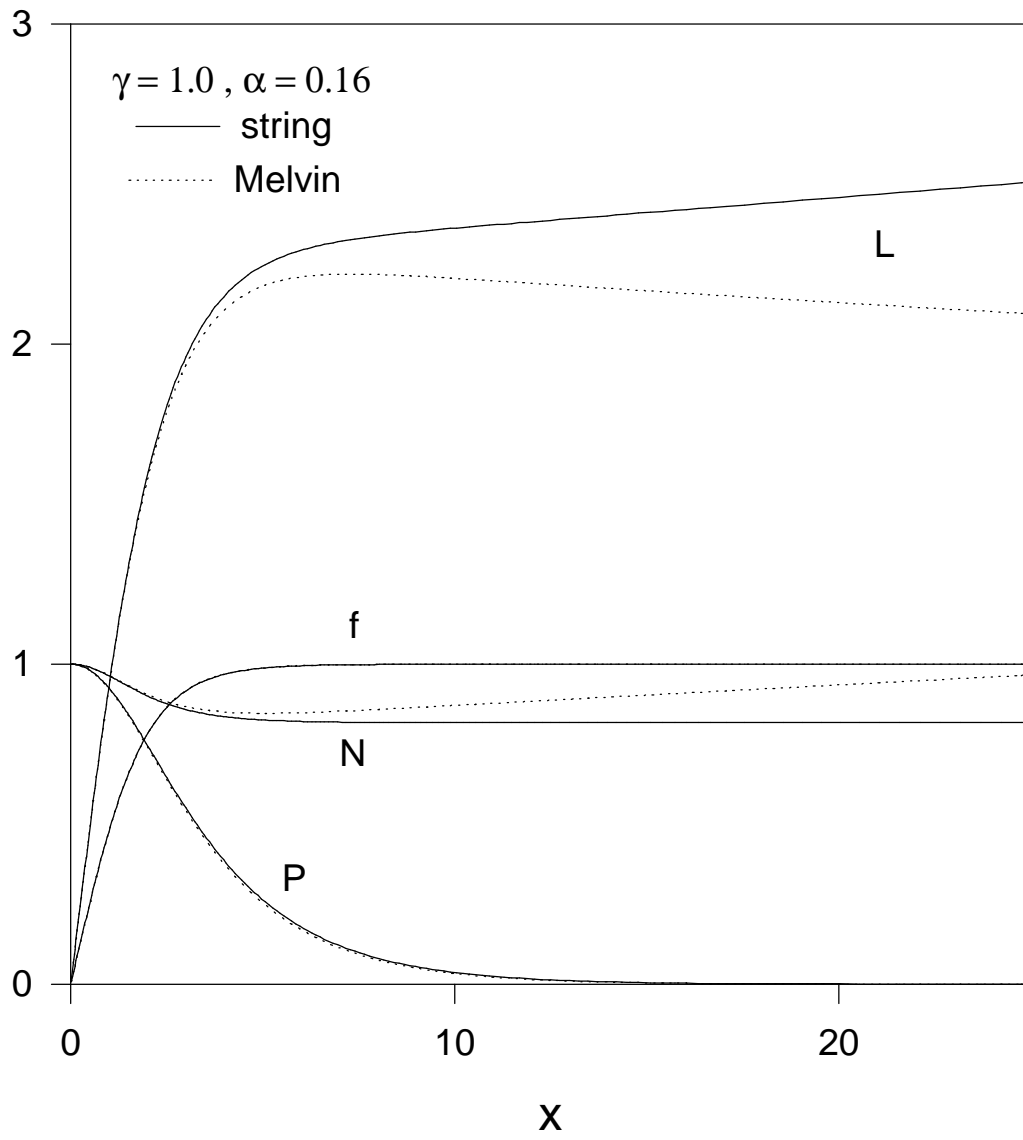


Figure 4





**Figure 5**



**Figure 6**

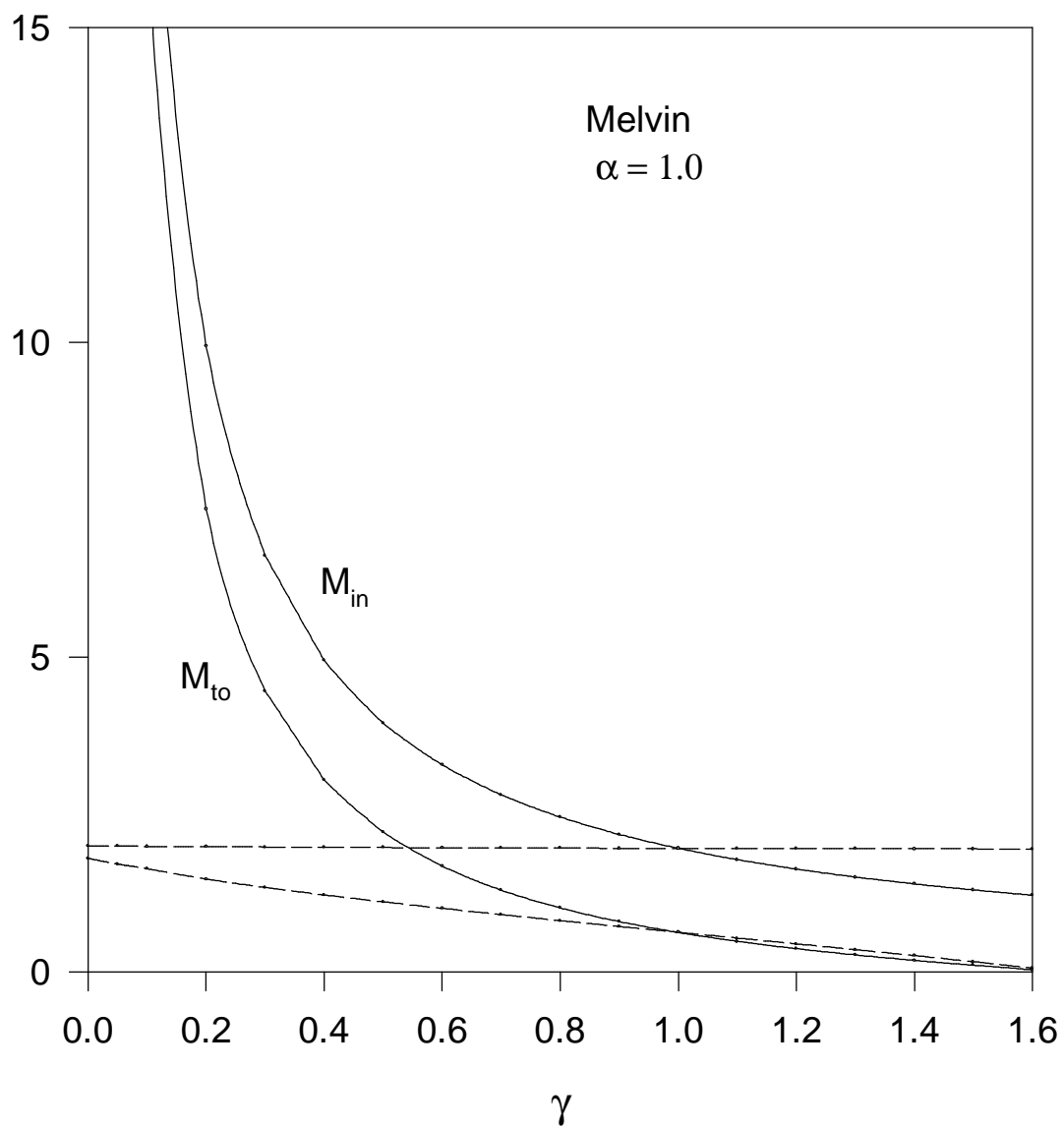


Figure 7

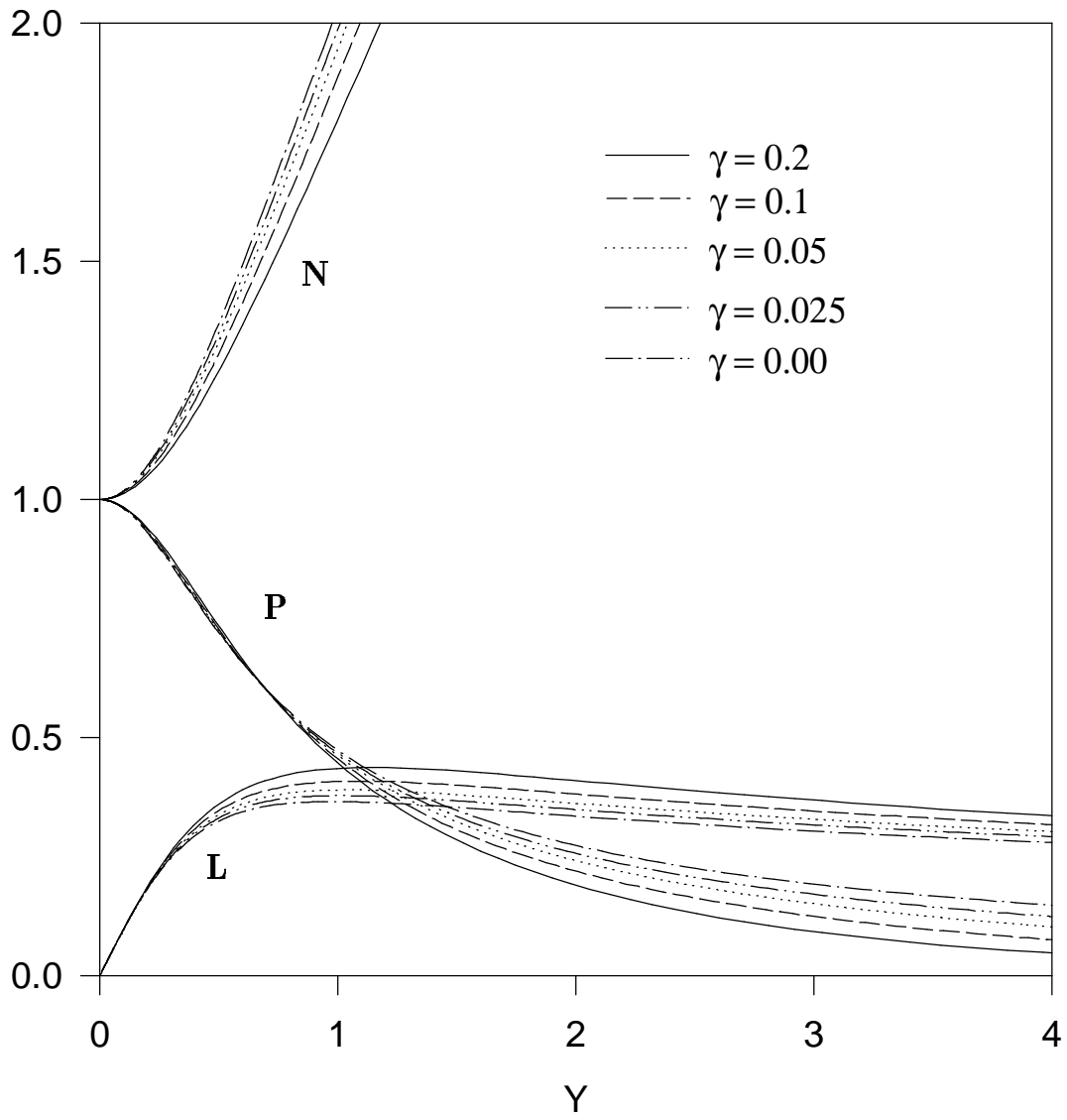
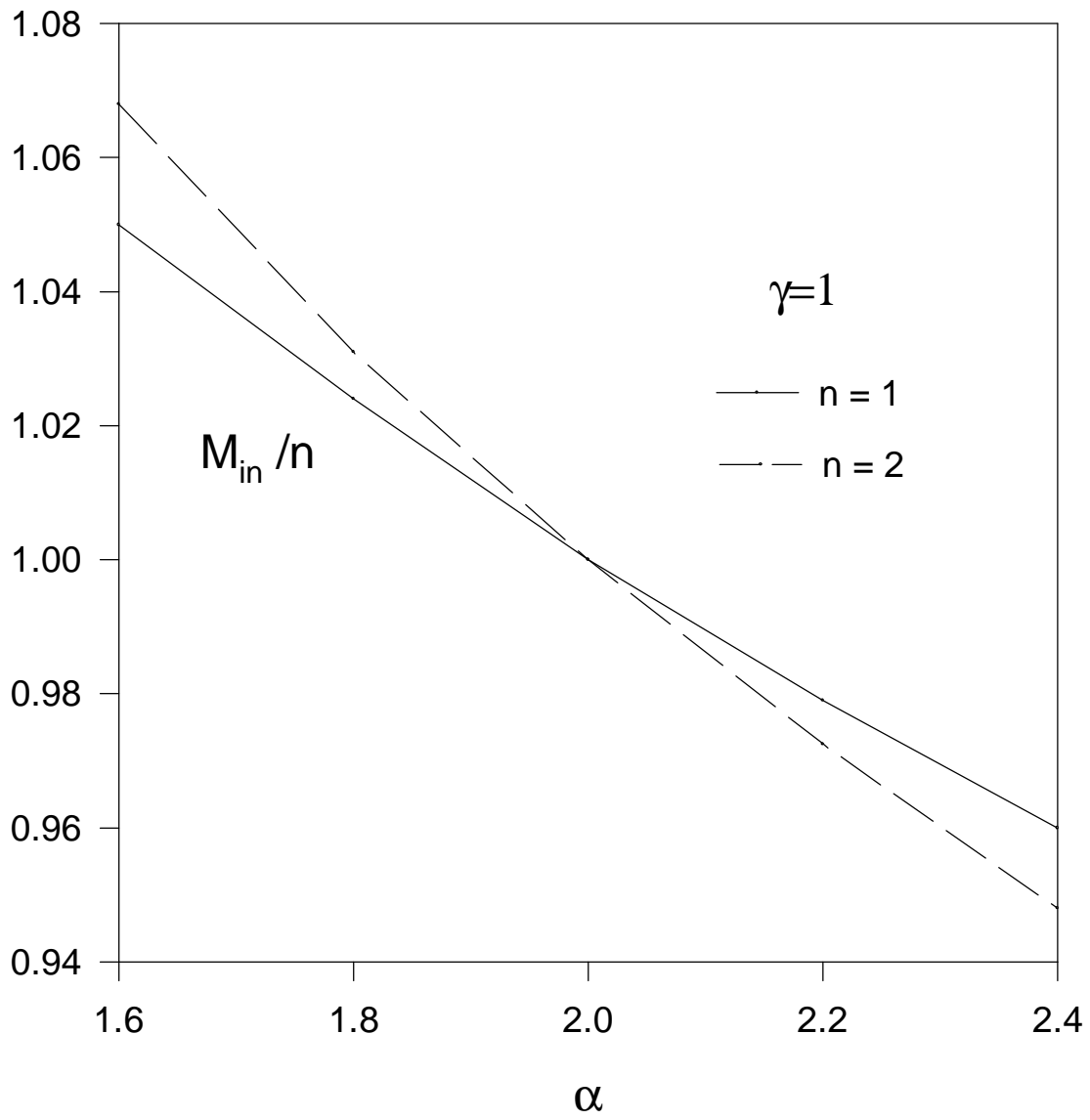


Figure 8



**Figure 9**

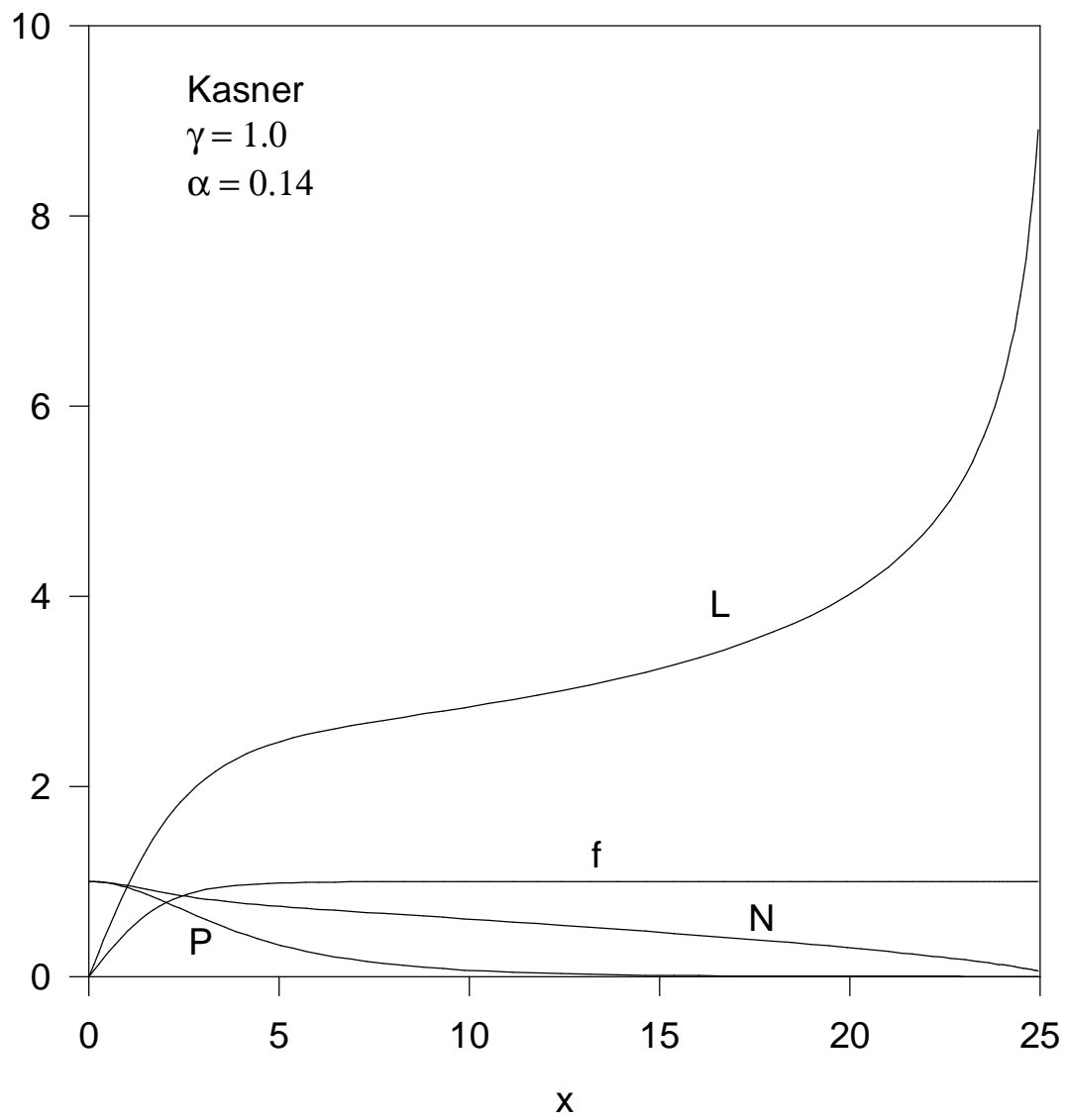


Figure 10

